EPR Characterisation of Bis(dimethylglyoximato)-Cobalt(II) Complexes and Their Oxygen Adducts Synthesised in an X-Zeolite Matrix

W. Lubitz

Institut für Organische Chemie, Freie Universität Berlin

C. J. Winscom

Institut für Molekülphysik, Freie Universität Berlin*

H. Diegruber and R. Möseler +

Institut für Angewandte und Physikalische Chemie, Forschungsgruppe Angewandte Katalyse, Universität Bremen**

Z. Naturforsch. **42a**, 970–986 (1987); received July 27, 1987***

The synthesis of bis(dimethylglyoximato)-cobalt(II) ($Co^{II}(dmgH)_2$) in the α-cages of a cobalt-exchanged sodium X-zeolite is described. A simple hydration/oxygenation sequence culminating in a superoxo complex, $Co^{III}(dmgH)_2 \cdot H_2O \cdot O_2^-$ has been studied using X-band EPR spectroscopy. The identification of the precursor species: square-planar $Co^{II}(dmgH)_2$, distorted $Co^{II}(dmgH)_2$ and $Co^{II}(dmgH)_2 \cdot 2H_2O$ was aided by comparison of their g- and ^{59}Co hyperfine tensor principal values with those of model complexes. On the basis of this identification the reaction sequence is discussed.

1. Introduction

Transition metal complexes formed in the large cavities of faujasite-type zeolites have recently received considerable attention because they offer interesting possibilities in both fundamental and applied catalysis [1–3]. For example, the intrinsic shape and cavity size of the zeolite matrix may be able to impose a selectivity upon an otherwise non-selective metal catalyst. Furthermore, the zeolite could modify the properties of the occluded complex as a result of different steric restraints and crystal field effects. Such complexes often show a behaviour different from that found in solution chemistry.

Co^{II} complexes comprise an interesting class of species which have been extensively studied to gain a better understanding of bonding and activation of molecular oxygen in biological and catalytic systems [4]. Various groups have succeeded in synthesising cobalt(II) complexes with different ligands in X- and Y-type zeolites, see e.g. [3, 5–17]. Several studies reported the behaviour of these complexes towards oxygen [8–11, 13–15]. Lunsford and coworkers found that bulkier ligands favour the formation of mononuclear complexes $Co^{III}O_2^-$, whereas in solution the binuclear species $Co_2^{III}O_2$ are much more common [9]. A particular problem with respect to catalytic usefulness was the stability of the superoxo-complex [11]. Recently Herron [15] has advanced the description of a "molecular ship in a bottle" for such complexes occluded in zeolite Y.

Our interest has focussed on the square-planar bis-(dimethylglyoximato)-cobalt(II) or cobaloxime(II) ($Co^{II}(dmgH)_2$) as an alternative. It is well-matched to the internal dimensions of an X-zeolite supercage and is a quite stable, neutrally charged complex (see Figure 1). Moreover, it is an interesting candidate for other reasons. Cobaloximes(II) are known to participate in a variety of organic reactions, where species with coordinated molecular H_2 [18] and O_2 [19, 20] have been postulated as reactive intermediates. $Co^{II}(dmgH)_2$ itself serves as a chemical model for vitamin B_{12r} and consequently has been well-studied in the last decade [21–24]. Its solution chemistry, and in particular details of its additional axial coordination, may be

+ Present address: Dräger Werke, D-2400 Lübeck.
* Arnimallee 14, D-1000 Berlin 33.
** D-2800 Bremen 33.
*** The first version was received in April 16, 1987.

Reprint requests to Prof. Dr. W. Lubitz, Institut für Organische Chemie, Freie Universität Berlin, Takustr. 3, D-1000 Berlin 33.

0932-0784 / 87 / 0900-0970 $ 01.30/0. – Please order a reprint rather than making your own copy.

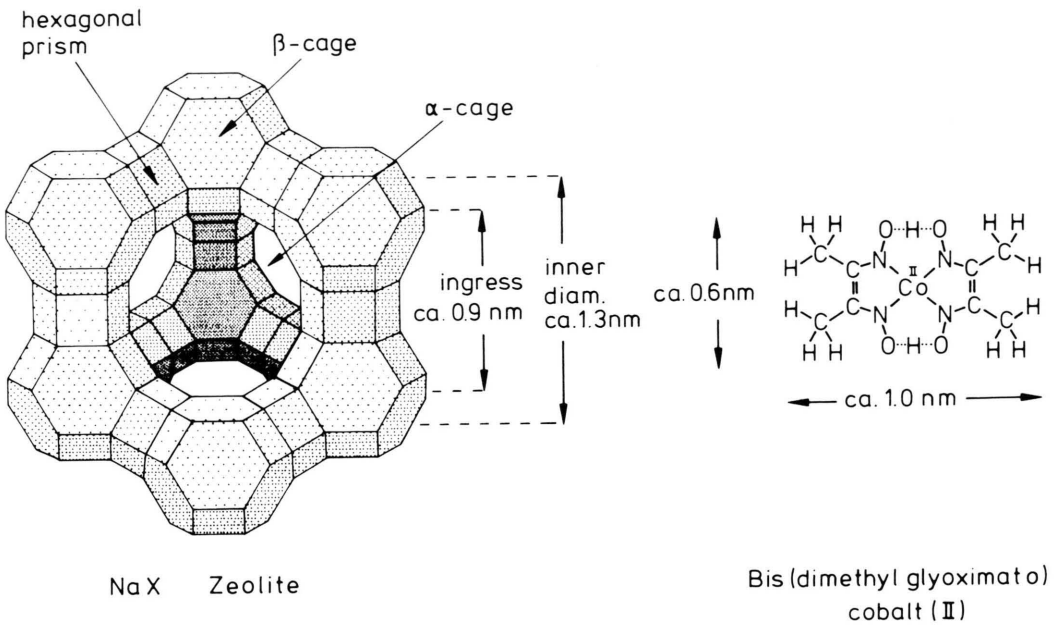

Fig. 1. Structure of the NaX zeolite lattice detailing the basic building blocks: the β- or sodalite-cages are connected by hexagonal prisms, thereby forming the large α-cages, also called "supercages". The inner diameter of the latter are ca. 1.3 nm, ingress to the α-cages is through windows of ca. 0.9 nm diameter. On the right, the structure of the $Co^{II}(dmgH)_2$ complex with overall dimensions is given; it is well-suited to fit into the center of the α-cages. For further details see text and [34], [32].

advantageously studied by EPR spectroscopy [22, 23, 25 – 28]. All the species involved have low-spin configured doublet ($S = 1/2$) ground states in which the unpaired electron resides in the Co $3d_{z^2}$ orbital ($z \perp$ to $Co^{II}(dmgH)_2$ plane). The spin Hamiltonian parameters of such ground states are thus extremely sensitive to changes in axial ligation.

In this work we describe the synthesis of $Co^{II}(dmgH)_2$ in a cobalt-exchanged NaX zeolite, and an X-band EPR study of the various species formed in the course of simple hydration and oxygenation sequences. In similar zeolite samples, such occluded $Co^{II}(dmgH)_2$ species exhibit the capability of selectively oxidizing propene, but suffer from rapid deactivation [29]. Apart from establishing the ultimate formation of a superoxo complex $Co^{III}O_2^-$, the main goal has been to characterise the immediate Co^{II} precursor species prior to the infusion-of-oxygen step. The characterisation relies on comparisons with model complexes formed in the absence of a zeolite environment, and a detailed analysis of the respective spin Hamiltonian parameters derived from their EPR spectra. A preliminary report of this work was given elsewhere [30, 31]. Additional and corroborative studies on these systems have been carried out by ESCA [32] and optical spectroscopy [33, 34].

2. Experimental

2.1 Preparation of the Zeolites

NaX zeolites with a ratio Si/Al = 1.1 and crystallite sizes ranging from 5 – 10 μm were synthesised following standard procedures of hydrothermal crystallization [35]. Triethanolamine was used as complexing additive [36]. The Si/Al ratio was determined by gravimetric (Si) and complexometric (Al) analyses as well as by X-ray fluorescence. Prior to ion exchange, the NaX was heated under shallow-bed conditions (air flow, 1 K/min to 673 K, 673 K for 5 h) to remove organic contaminants. After cooling to room temperature (RT), the NaX was rehydrated by placing it over a saturated KCl solution prior to use.

Ion-exchange was carried out in solutions of cobalt acetate ($Co(CH_3COO)_2$, Merck p.A.) at

room temperature where a uniform dispersion was obtained by continuous shaking. The desired degrees of exchange (5.1% and 15.7%) were achieved by eluting the NaX powder with solutions of $Co(CH_3COO)_2$ ($0.005\ M \cdot l^{-1}$ and $0.017\ M \cdot l^{-1}$, respectively). Higher degrees of exchange, namely 35%, were achieved by successive exchange procedures. All the samples were washed anion-free, air dried and stored over a saturated KCl solution in a desiccator. The complete uptake of the cobalt by the zeolite was determined by atomic absorption spectrometry (AAS) of the filtered solution and of the cobalt zeolite. For the latter determination, the minerals were dissolved in hydrochloric acid (HCl, 0.1 N). Standard solutions for calibration were prepared from solutions of cobalt chloride ($CoCl_2$) in HCl by adding adequate amounts of NaX to account for the matrix effect. A mean relative error of 5% was found for these determinations. Since the ion-exchange was carried out at a $pH \approx 5$, no precipitation of cobalt hydroxides at the external surface of the zeolite crystals by hydrolysis occurred.

The exchanged zeolites were designated $Co_{2.3}NaX$ (5.1% exchange), $Co_{7.2}NaX$ (15.7%) and $Co_{16.1}NaX$ (35%); the respective subscripts indicate the number of Co^{II} ions per unit cell. These correspond to an average of 0.3, 0.9, 2.0 possible Co^{II} ions per supercage, respectively, assuming complete Co^{II} exchange.

Zeolite samples were dehydrated by heating to 653 K in increments of 1 K/min in a purified Argon flow (held at 653 K for 7 h). Samples described in later sections, which were derived from the Co-exchanged NaX followed by this dehydration step, will be denoted by a = anhydrous, e.g. $Co_{7.2}NaX$ (a).

2.2 Preparation of Samples A – E

In the following, quantitative details are given for $Co_{7.2}NaX$; for $Co_{2.3}NaX$ and $Co_{16.1}NaX$ the conditions and quantities were almost identical. Each sample was sealed under reduced pressure (10^{-3} mbar).

The ligand dimethylglyoxime, $dmgH_2$, (Merck, p.A.) was predried by pumping (10^{-3} mbar) at RT and 323 K for 2 h at each temperature. The dehydrated $Co_{7.2}NaX$ (ca. 3 g) and $dmgH_2$ (ca. 1 g) were then respectively filled into the individual compartments of a two chamber reaction vessel under argon. Following the evacuation to ca. 10^{-5} mbar, the glass ampoule was sealed and the $dmgH_2$ then allowed to infuse into the $Co_{7.2}NaX$ at 373 K for 70 h with frequent shaking of the zeolite bed to ensure homogeneity. When the reaction product appeared to be homogeneous (sample A), the zeolite chamber was sealed off under inert conditions. The adsorption of $dmgH_2$ was quantitatively determined by chemical analysis.

Bidistilled water was deoxygenated by bubbling with purified Ar gas at RT for 4 h. Part of sample A was hydrated at RT in a pure-water-vapor-saturated Ar atmosphere for 15 h and then evacuated for 2 h (10^{-3} mbar) to desorb the excess water (sample B).

Part of sample B was then exposed to oxygen (1 bar), which had been prepurified in a zeolite-A trap, and allowed to adsorb at RT for 4 h (sample C).

In a second series of experiments the last two steps of the reaction pathway (hydration and oxygenation) were reversed. Here, sample D designates the reaction product resulting from the interaction of sample A with oxygen, whereas sample E is the following hydrated one.

2.3 Preparation of the Model Systems

For characterisation of the different species present in the zeolite samples it was found useful to refer to two model systems, namely $Co^{II}(dmgH)_2$ diluted in $Ni^{II}(dmgH)_2$ as a co-crystallized powder [37, 28] and $Co^{II}(dmgH)_2$ in a frozen water solution, which was prepared following Schrauzer and Windgassen [24].

2.4 EPR Spectrometer

The EPR measurements were performed on an X-band spectrometer comprising an AEG X-20 magnet and a Bruker ER 200 D mainframe, which provided a 100 kHz field modulation. A rectangular Bruker cavity was used, into which a quartz nitrogen gas flow cryostat regulated by a Bruker 4111 VT temperature control unit was installed. All spectra were recorded at a sample temperature of 120 K, unless otherwise stated. The magnetic field was stabilized by using a Hall effect probe and measured with an NMR gaussmeter (AEG GA

EPR 11/21). The microwave frequency was determined by a HP 5340A frequency counter. The experimental conditions used are outlined in the respective figure legends.

2.5 Simulation of EPR Spectra

The program used to simulate frozen glass spectra required only the handling of doublet ($S = 1/2$) electronic states and one nuclear spin ($I \leqq 7/2$) The spin Hamiltonian employed was

$$\mathcal{H} = \beta_e \boldsymbol{B}_0 \cdot \mathbb{g} \cdot \boldsymbol{S} + \boldsymbol{S} \cdot \mathbb{A} \cdot \boldsymbol{I},$$

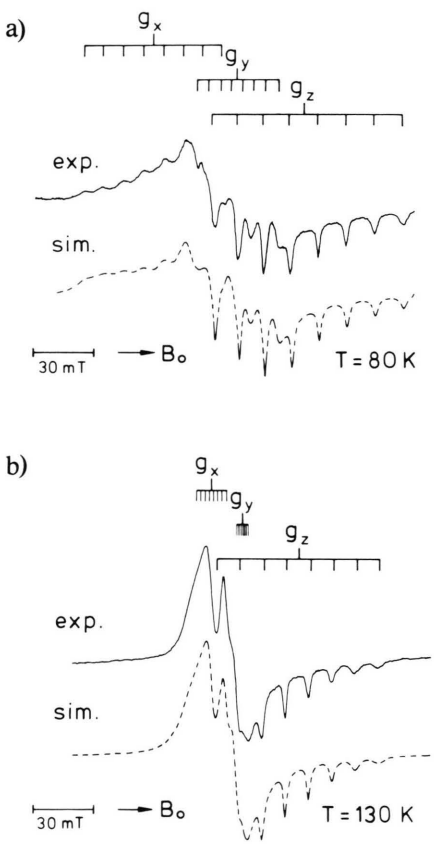

Fig. 2. Experimental and simulated spectra of $Co^{II}(dmgH)_2$ in (a) a $Ni^{II}(dmgH)_2$ cocrystallized powder and (b) frozen water. The principal g-tensor values and the hf splitting due to the ^{59}Co nucleus ($I = 7/2$) are indicated (see Table 1). The spectrum obtained in the Ni^{II} host was kindly provided by A. Schweiger, ETH Zürich [37]; we have repeated this experiment and obtained similar values [28]. Spectrometer settings (b): X-band, 100 kHz field modulation: depth 10 G, microwave power 30 mW, single scan (500 s) with a time constant 0.5 s.

where β_e is the Bohr magneton, $\boldsymbol{B}_0$ the magnetic field, $\mathbb{g}$ the g tensor and $\mathbb{A}$ the electron-nuclear dipolar hyperfine tensor. In none of the specta was it found necessary to account for second order effects arising from inclusion of a quadrupole term. A treatment similar to that given by Bleaney [38], but allowing for orthorhombic g- and A tensors with coincident principal axes [39], has been adopted to determine the orientation dependent resonance fields, B_m (l, m, n) where l, m, n are the direction cosines with respect to the principal g-and ^{59}Co hf tensors axis system. Consistently better fits were obtained by adopting a Lorentzian-rather than a Gaussian-lineshape, in contrast to the studies of Rockenbauer and Simon [40] and others [41, 42]. A significant m_I and m_I^2 linewidth dependence was apparent. Accordingly, a Lorentzian lineshape with width given by

$$\Delta B(m_I) = U + V m_I + W m_I^2$$

was adopted where $U(l, m, n) = (l^2 U_x^2 + m^2 U_y^2 + n^2 U_z^2)^{1/2}$ and analogous expressions for V and W were used [42]. For paramagnetic species in polycrystalline or zeolite hosts, the main linewidth contributions are: local crystal field variations [41, 42] and restricted motion giving rise to correlation effects similar to those in solution [43].

3. Results

3.1 Model Complexes

3.1.1 $Co^{II}(dmgH)_2$ in $Ni^{II}(dmgH)_2$

The EPR spectrum of $Co^{II}(dmgH)_2$ in $Ni^{II}(dmgH)_2$ and its simulation are shown in Figure 2a. The spectrum comprises three eight-line hyperfine splitting (hfs) patterns resulting from a markedly orthorhombic g tensor and an anisotropic ^{59}Co hfs tensor (^{59}Co: $I = 7/2$). The respective principal values are listed in Table 1. In each eight-line hfs pattern the simulation requires a linewidth variation for the different nuclear spin components of the pattern (see Section 2.5). Furthermore, between the differently centred hfs patterns the magnitudes of the linewidth parameters are quite different. This feature was found to be common for all the Co^{II} species discussed in this paper.

Table 1. Principal values of the g- and ^{59}Co hyperfine[a] tensors for the $Co^{II}(dmgH)_2$ complexes.

	Model Compounds		Zeolite Species		
	$Co^{II}(dmgH)_2$ in $Ni^{II}(dmgH)_2$	$Co^{II}(dmgH)_2$ in H_2O	Species 1 sample A	Species 2 samples B, C, E	Species 3 samples B, E
g_x	2.595	2.310	2.543	2.605	2.312
g_y	2.245	2.194	2.262	2.196	2.190
g_z	1.995	2.009	2.003	1.980	2.009
$\lvert A_x \rvert$ [b]	370	70	252	336	126
$\lvert A_y \rvert$ [b]	185	20	114	132	27
$\lvert A_z \rvert$ [b]	378	328	315	348	338

[a] in MHz.
[b] EPR determines only the magnitudes of the ^{59}Co hf principal values. However, for all reasonable variations of the proposed Co^{II} ground state, theory (see text) predicts that all components are positive.

3.1.2 $Co^{II}(dmgH)_2$ in water

In Fig. 2b, the experimental EPR spectrum of $Co^{II}(dmgH)_2$ in a frozen solution of pure water is presented together with its simulation. The principal values of the g- and ^{59}Co hfs tensors used for the simulation are given in Table 1. The main differences compared with the $Ni^{II}(dmgH)_2$ host are the more cylindrical characters of both tensors. This can be readily explained on the basis of the different axial coordination in the two hosts, and will be dealt with in greater detail in the following section. In view of the significant linewidths and relatively small ^{59}Co hfs along the in-plane principal axes (x, y) much of the hyperfine structure is lost.

A similar EPR experiment was performed in methanol instead of water (not shown here) [28]. The basic characteristics are found to be very similar with the spin Hamiltonian parameters: $g_x = 2.300$, $g_y = 2.191$, $g_z = 2.012$, $A_x = 45$ MHz, $A_y = 20$ MHz, $A_z = 310$ MHz at 140 K, and in solution $g_{iso} = 2.194$, $A_{iso} = 165$ MHz at 275 K. We differ from the conclusion of Rockenbauer *et al.* [27] in so far as we found it necessary to retain *orthorhombic* g- and ^{59}Co hfs tensors for a satisfactory simulation.

3.2 Complexes in the X-Zeolite Matrix

The samples derived from $Co_{7.2}NaX$ correspond to approximately one complex per available supercage (α-cage). Unless otherwise stated the spectra presented here are derived from $Co_{7.2}NaX$. Assignment of the various species to mononuclear Co^{II}-complexes was for some samples tested by comparison with the $n = 2.3$ and/or $n = 16.1$ analogues. This allowed a check on the possible aggregation of Co^{II} ions and subsequent formation of bicobalt complexes. This procedure is especially relevant for those samples where cobalt-oxygen complexes are expected.

3.2.1 Control samples

The following samples were examined under the same EPR conditions as for the Co^{II}-exchanged samples: a) pure NaX zeolite, b) as a) but loaded with $dmgH_2$, and c) as b) with infusion of oxygen. In no case was an EPR signal observed in the range 0.2 – 0.4 T between 100 K to 300 K.

3.2.2 $Co_{7.2}NaX$, dehydrated ($Co_{7.2}NaX(a)$)

The Co^{II}-exchanged zeolites after dehydration were examined by EPR above 100 K. The sample exhibited a very broad asymmetric signal (0.2 – 0.3 T) centred at approximately 0.15 T. This was attributed to high spin ($S = 3/2$) Co^{II} ions, in accordance with the observations of Mikheikin *et al.* [44, 45].

3.2.3 Sample A ($Co_{7.2}NaX$ (a, $dmgH_2$))

The infusion of $dmgH_2$ into $Co_{7.2}NaX(a)$ yielded the same broad $S = 3/2$ signal as in the foregoing sample, but with a slightly reduced intensity. Additionally, new, sharper features appeared in the $g \approx 2$ region. A coarse comparison of the integrated intensities of the broad and the sharply structured signals in sample A with that in $Co_{7.2}NaX(a)$ indicates that the $g \approx 2$ signals are

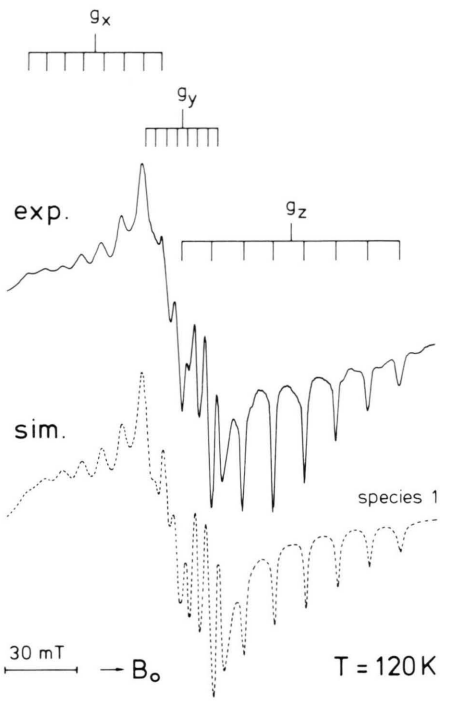

Fig. 3. Experimental (top) and simulated (bottom) EPR spectra obtained from species 1 (see text) in the zeolite sample A at 120 K, for other conditions see Fig. 2. The principal g and ^{59}Co hfs values are indicated the data are given in Table 1.

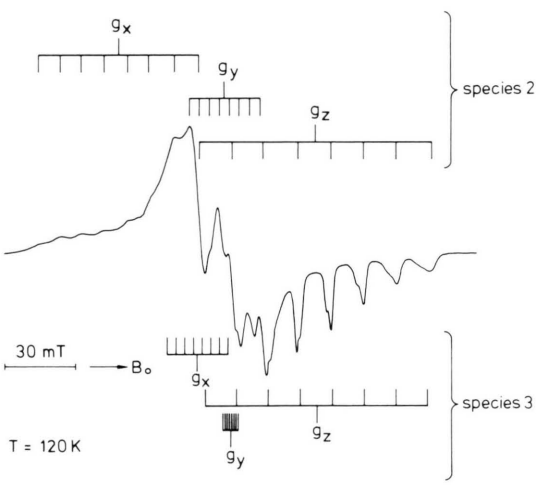

Fig. 4. EPR spectrum obtained from sample B at 120 K showing a superposition of signals from species 2 and 3 (see text), the principal g- and ^{59}Co hfs values are indicated for both complexes. Some small features from species 1 are also present in this incompletely hydrated sample. The spectrometer settings were similar to those used for sample A and the model compounds. For simulations of the individual EPR spectra of species 2 and 3 see Figures 5 and 7, respectively; the data are collected in Table 1.

born at the expense of 10 – 20% of the broad $S = 3/2$ species. Figure 3 shows the details of the $g \approx 2$ region. The g tensor anisotropy and the sharp ^{59}Co hfs features are entirely consistent with a low-spin ($S = 1/2$) Co^{II}-complex. For chemical reasons [46], it was expected that a Co^{II}-complex in which two (dmgH)-ligands take a square planar arrangement about the Co^{II} ion would be formed.

The spin Hamiltonian parameters used to simulate the EPR spectrum of this complex (hereafter referred to as species 1) are given in Table 1. The EPR spectrum shown in Fig. 3 shows a small contamination from a secondary low spin species, referred to as species 2, with an integrated intensity of ca. 10% of species 1.

3.2.4 Sample B ($Co_{7.2}NaX$ (a, $dmgH_2$, H_2O))

The infusion of water into sample A produced significant changes in the observed EPR spectrum. The previously observed high-spin Co^{II} species was almost completely absent, whereas the more sharply featured signals in the $g \approx 2$ region significantly increased in their intensity compared with those of sample A. The $g \approx 2$ region is shown in Figure 4. Two different Co^{II} species, species 2 and a new species referred to as species 3, are primarily responsible. The relative proportion of species 2 to 3 is ca. 1 : 2 (from EPR simulation and superposition of spectra). Species 1 is also present in trace amounts.

A deconvolution of the signals arising from species 1 – 3 was possible by infusion of an excess of water, yielding predominantly one species (species 3) and only a small contamination from species 2. In this sequence of experiments the "growing in" of species 3 at the expense of species 2 could be easily followed. The spin Hamiltonian parameters of the two species derived from separate simulations (see also sample C below) are given in Table 1.

3.2.5 Sample C ($Co_{7.2}NaX$ (a, $dmgH_2$, H_2O, O_2)

Exposure of Sample B to oxygen showed a further marked change in the $g \approx 2$ spectral region, which is depicted in Figure 5. The spectrum comprises two distinct species. One of the species (species 2) may be clearly identified as being present in sample B with approximately the same signal intensity. The simulated spectrum of species

2 is shown in Fig. 5 (bottom) yielding the spin Hamiltonian parameters listed in Table 1. The second species shown as an insert in Fig. 5 must be formed from species 3 (see sample B) under conditions of oxygen infusion. This spectrum may also be simulated (see Fig. 5, insert); the spin Hamiltonian parameters required are quite different from these found in the other low-spin cobalt species so far and are:

$$g_1 = 2.052, \quad |A_1| = 42.9 \text{ MHz},$$
$$g_2 = 2.015, \quad |A_2| = 33 \text{ MHz},$$
$$g_3 = 1.986, \quad |A_3| = 36 \text{ MHz}.$$

All three principal g-values lie closer to the free electron g-value, and the ^{59}Co hfs principal values are markedly reduced in magnitude and almost isotropic. The spectral appearance of this species (species 4) clearly demonstrates the existence of a cobalt superoxo complex [4] in sample C. The simulated spectrum shows minor departures from the experimental one arising from the superposition of broader features originating from species 2.

In this sample further infusion of water causes additional formation of species 3 from species 2. Subsequent exposure to oxygen increases the concentration of species 4 formed from species 3. No evidence could be found for direct conversion from species 2 to species 4. Species 4 is quite stable and does not lose its oxygen under evacuation at RT.

3.2.6 Sample D ($Co_{7.2}NaX$ (a, $dmgH_2$, O_2)

The sequence of samples A, B, and C forms one synthetic aspect of $Co^{II}(dmgH)_2$ complex formation within the zeolite. When sample A is exposed to oxygen under strictly anhydrous conditions, the residual high-spin Co^{II} signal remains almost unchanged whereas species 1 disappears completely and is replaced by the appearance of the signal (species 5) shown in Figure 6. Species 5 is stable to subsequent evacuation. Its spectrum is centred about the free electron g-value and comprises a number of narrowly spaced lines, whose widths are $\leqq 10^{-3}$ T. The typical features of a ^{59}Co hfs patterns are completely absent. Furthermore, this species was easier to saturate than all the other species observed and could even be detected at RT without significant loss in resolution. Attempts to simulate its spectrum, on the basis that the unpaired electron interacts anisotropically with a single nuclear spin of $I = 1/2$, 1 or 5/2, and that the g- and hfs tensors have collinear principal axes, proved unsatisfactory. It is most nearly reproduced with a single nucleus $I = 1$ and we suggest that non-collinear g- and hfs tensor axes are the main cause of the discrepancy. Moreover, it is like-

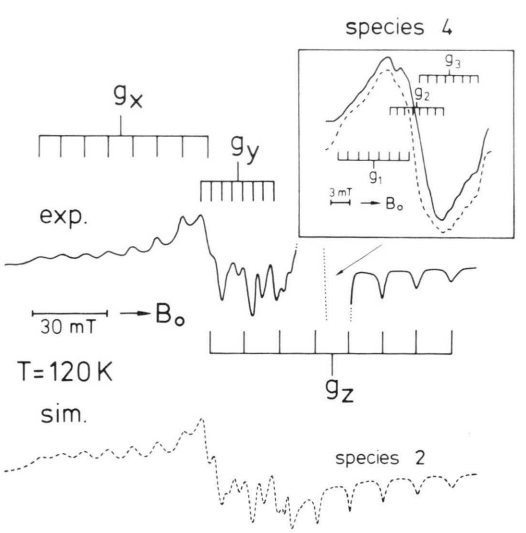

Fig. 5. Experimental EPR spectrum of sample C (top) at 120 K showing features from species 2 (simulation at bottom) and from species 4 (see insert). For both species the principal g- and ^{59}Co hfs values are indicated, for data see Table 1 and text. The spectrometer settings are given in Fig. 2; for species 4 (insert) mw power 20 mW, mod. depth 5 G, time constant 1 s was used.

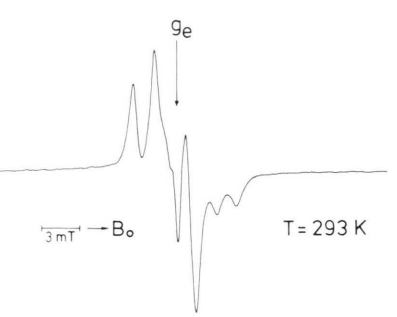

Fig. 6. EPR spectrum of sample D showing species 5 at RT. The spectrum is similar at 120 K but somewhat less resolved. The free electron g value is indicated. Note the narrow width of the spectrum typical for an organic radical. Spectrometer settings: 100 kHz mod. depth 2.5 G, mw power 25 mW, other settings as in Figure 2.

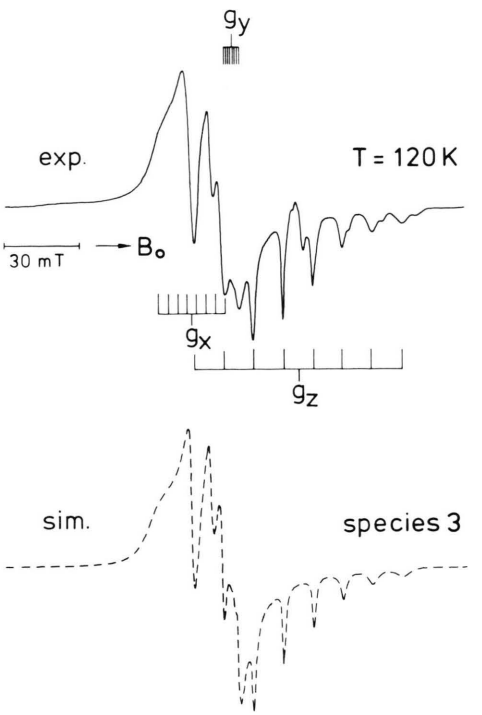

Fig. 7. Experimental EPR spectrum obtained from sample E. It shows features from species 2, 3 and 5, for the dominant one (species 3) the g- and ^{59}Co hf-values are indicated and the simulation is shown (bottom). The remaining species 5 appears as small line near $g \approx 2 \approx g_z$ in the upper trace. For spectrometer settings see Figure 2.

ly that a secondary paramagnetic species centered at ca. g_e is superimposed on the main signal which further frustrates a satisfactory simulation.

3.2.7 Sample E ($Co_{7.2}NaX$ (a, $dmgH_2$, O_2, H_2O))

Addition of water vapor in an argon stream to sample D yields the spectrum shown in the upper part of Fig. 7 (sample E). This spectrum is similar to that of sample B (Fig. 4) but with significant retention of species 5. By changing the duration of exposure to water, species 2 and 3 could be obtained in different proportions than those shown in Fig. 4 for sample B. The spectrum shown in Fig. 7 is for conditions under which species 3 is dominant; a simulation using the parameters given in Table 1 is presented in the lower part of the figure for comparison. Clearly, the water serves to free the remaining high spin Co^{II} in tetrahedral sites [44, 45], which then complexes with residual $dmgH_2$ to form species 2 and 3. Surprisingly, species 5 remains quite stable to hydration. Additional infusion of oxygen to sample E results in a conversion of species 3 to the superoxo complex (species 4), as expected, which is then superimposed on the weaker signal of species 5.

4. Discussion

4.1 Theory

The low-spin Co^{II} species in this work all contain the square planar $Co^{II}(dmgH)_2$ unit and differ in their axial coordination. For discussion of the spin Hamiltonian parameters it is useful to refer to a diagram of the level ordering for the relevant molecular orbitals (mo's). Such a scheme is shown in Figure 8.

The EPR data of all the precursor Co^{II} species, excluding those involving Co^{II} ions in tetrahedral sites and the Co^{III} species involving O_2^-, confirm that they have doublet ($S = 1/2$) ground states and that the unpaired electron (upe) resides in an mo having mainly d_{z^2} character. The principal values of the g tensor and ^{59}Co hfs tensor of these Co^{II} species may be analysed to yield the spin density distribution in the metal orbitals and a reliable energetic placement of low-lying metal-based excited states. Using a nomenclature consistent with the C_{2v} point group, McGarvey [47] has given expressions for the important spin Hamiltonian parameters for the various doublet ground state possibilities, which will be valid [47, 48] provided that the anisotropic g-shifts are not excessive. For species studied in this work, this is the case since the largest shift observed is 0.6. The expressions given in reference [47] for a $^2A_1$: $(a\,d_{x^2-y^2} - b\,d_{z^2})^2 \cdot (d_{xz})^2\ (d_{yz})^2 (d_{z^2})^1$ ground state are adopted; two minor modifications to account for d-orbital mo coefficients, i.e. α_1, α_2, β_1, β_2, γ in Fig. 8, less than 1.0 are made. The spin orbit interaction parameters: c_1, c_2, ..., c_3', c_4' used by McGarvey are retained but their definitions become, for example, $c_1 = \alpha_1^2 \beta_1^2 \zeta / \Delta E_1(^2B_1)$, etc., where ζ is the spin-orbit coupling constant for the Co^{II} ion and ΔE_1 is the energy separation between the ground state and the relevant singly excited state. Coefficients c_3, c_4 involve energy separations to quartet excited states and c_3', c_4' the corresponding higher-

lying doublet counterparts. Secondly, the purely dipolar terms in the expressions for the principal ^{59}Co hfs values are correspondingly modified, for example the dipolar part of A_z becomes $\frac{4}{7}P(a^2-b^2)\alpha_1^2$, where $P = g_N\beta_N g_e\beta_e\langle r^{-3}\rangle_{3d}$ for Co^{II}. Throughout this work the values $\zeta = 515\ cm^{-1}$ [49] and $P = 220\cdot 10^{-4}\ cm^{-1}$ [50] for the complexed Co^{II} ion will be adopted as constants.

McGarvey's derivation is taken to third order in perturbation theory; when all the terms are retained the expressions become unwiedly. The following approach is therefore adopted to enable a sensible truncation to be made. By making appropriate substitutions involving Δg_x and Δg_y to account for the leading second order terms involving the most critical coefficients, c_1 and c_2, the expressions become

$$\Delta g_x + \frac{1}{12}(\Delta g_y^2 + \Delta g_x \Delta g_y) = 2(|\sqrt{3}a+b)^2 c_2 + \frac{2}{3}c_3^2, \quad (1)$$

$$\Delta g_y + \frac{1}{12}(\Delta g_x^2 + \Delta g_x \Delta g_y) = 2(|\sqrt{3}a-b)^2 c_1 + \frac{2}{3}c_4^2, \quad (2)$$

$$\Delta g_z + \frac{1}{12}(\Delta g_x^2 + \Delta g_y^2 - \Delta g_x \Delta g_y) = \frac{2}{3}(c_3^2 + c_4^2 + c_3 c_4), \quad (3)$$

$$A_x - P\left(\Delta g_x + \frac{1}{14}\Delta g_y\right) = K + P\left\{\left[-\frac{2}{7}(a^2-b^2) - \frac{4|\sqrt{3}}{7}ab\right]\alpha_1^2 + \frac{2}{7}(c_3 - c_3')\right\}, \quad (4)$$

$$A_y - P\left(\Delta g_y + \frac{1}{14}\Delta g_x\right) = K + P\left\{\left[-\frac{2}{7}(a^2-b^2) + \frac{4|\sqrt{3}}{7}ab\right]\alpha_1^2 + \frac{2}{7}(c_4 - c_4')\right\}, \quad (5)$$

$$A_z + P\left(\frac{1}{14}\Delta g_x + \frac{1}{14}\Delta g_y\right) = K + P\left\{\frac{4}{7}(a^2-b^2)\alpha_1^2 - \frac{2}{7}(c_3 - c_3') - \frac{2}{7}(c_4 - c_4')\right\}, \quad (6)$$

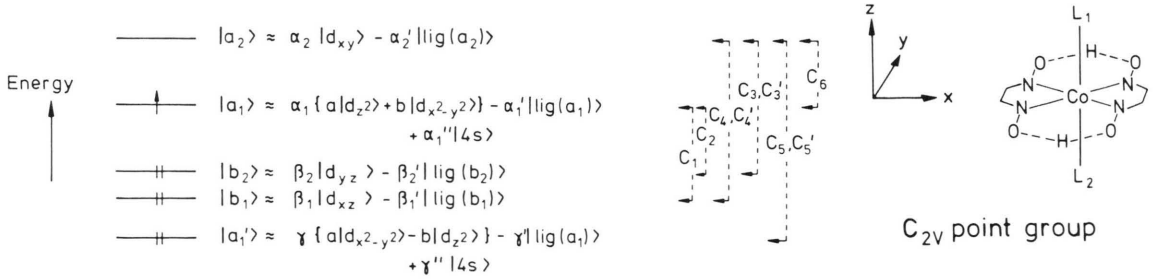

Fig. 8. Orbital level scheme for four- and six-coordinated low-spin Co^{II} complexes. The mo's are denoted by their corresponding irreducible representations according to C_{2v} point group symmetry. The relevant admixtures of 3d- and 4s-orbitals as well as ligand orbitals are given. The parameters c_1 to c_6 indicate the spin orbit interactions and correspond to those given by McGarvey [47] (see text). Coefficients c_6 and c_5, c_5' could be safely neglected; $c_1 \ldots c_4$ connect pairs of levels involved in single-excitations to form doublet- or quartet excited states; the important doublet- (ΔE_1, ΔE_2) and quartet- (ΔE_3, ΔE_4) excitation energies (see Table 2) are correspondingly correlated to the level pairs. The principal axes of the g tensor correspond to the molecular axes given in the diagram. The assignment of the in-plane principal axes was achieved by orientationally-selected ENDOR spectroscopy on $Co^{II}(dmgH)_2$ model complexes [28].

where $\Delta g_i = g_i - g_e$ (i = x, y, z) and K is the isotropic Fermi contact contribution to the hfs (see below).

The equations (1) to (6) are so arranged that the right-hand side of each contains only simple expression involving the crucial unknown coefficients K, α_1, a, b, c_1, ..., c_4, c_3' and c_4'. Additional relationships are required for the estimation of all these coefficients. Firstly, from the definitions in Fig. 8:

$$a^2 + b^2 = 1 . \tag{7}$$

Secondly, the coefficients c_1, c_2 are related to c_3, c_4. Since for the following Coulomb (J) and exchange (K) integrals, the following equalities for unperturbed metal 3d-orbitals [51] hold:

$J(xz, \mu) \equiv J(yz, \mu)$ and $K(xz, \mu) \equiv K(yz, \mu)$

$\mu = z^2, x^2-y^2, xy$ then

$\Delta E_3(^4B_1) - \Delta E_4(^4B_2) \approx \Delta E_2(^2B_2) - \Delta E_1(^2B_1)$.

Recalling the definitions of the c_j's, and assuming $\alpha_1 = \alpha_2$,

$$\frac{1}{c_1} - \frac{1}{c_2} \approx \frac{1}{c_4} - \frac{1}{c_3} . \tag{8}$$

Using similar arguments $\Delta E_3(^4B_1) - \Delta E_3'(^2B_1(1,2)) = \Delta E_4(^4B_2) - \Delta E_4'(^2B_2(1,2)) = E'$. McGarvey [47] has estimated that E' is about 15,000 cm^{-1}. This leads to the relations

$$c_3' = c_3/(1+fc_3); \quad c_4' = c_4/(1+fc_4) , \tag{9}$$

where $f = E'/\alpha_1^2\zeta$, (10)

taking note of later remarks regarding the calculation of excitation energies.

The crucial coefficients may now be fully determined. To complete the metal orbital spin-density analysis, the metal 4s information may be derived from the Fermi contact interaction, K. Since the $^2A_1$ ground state allows direct admixture of the metal 4s orbital, it comprises two contributions:

$$K = K_d \alpha_1^2 + K_s \alpha_1''^2 , \tag{11}$$

where for the Co^{II} ion $K_d = -85 \cdot 10^{-4}\,cm^{-1}$ [52] and $K_s = +1220 \cdot 10^{-4}\,cm^{-1}$ [53]. Equation (11) serves to enable the determination of $\alpha_1''^2$.

The excitation energies of the four relevant low-lying excited states (see Fig. 8) may now be estimated from the coefficients $c_1 \ldots c_4$. 3d-orbitals admixing ligand functions as a result of σ-overlap are assumed to have equal admixture coefficients (i.e. α_2, $\gamma \approx \alpha_1$), whereas those admixing with ligand π-orbitals are assumed to have coefficients equal to unity, owing to the smaller overlap (i.e. β_1, $\beta_2 \approx 1$).

The 3d, 4s metal orbital spin densities and the excited state energies for the model compounds and precursor species are presented in Table 2.

Table 2. The metal orbital spin densities and low-lying excited state energies of the model compounds and zeolite precursor species.

	Model Compounds		Zeolite Species		
	$Co^{II}(dmgH)_2$ in $Ni^{II}(dmgH)_2$	$Co^{II}(dmgH)_2$ in H_2O	Species 1 sample A	Species 2 samples B, C, E	Species 3 samples B, E
ϱ_{3d} [a]	0.84	0.91	0.88	0.78	0.87
ϱ_{4s} [a]	0.09	0.07	0.07	0.08	0.08
$\Delta E_1(^2B_1, xz \rightarrow z^2)$ [b]	8800	13500	8800	9800	13700
$\Delta E_2(^2B_2, yz \rightarrow z^2)$	4500	9400	5200	4200	8600
$\Delta E_4(^4B_2, xz \rightarrow xy)$ [c]	8000	8700	7100	18800	9300
$\Delta E_3(^4B_1, yz \rightarrow xy)$ [c]	3700	4600	3500	13200	4200

[a] In all cases $|a| \approx 1$, $|b| \leq 0.06$ (see text), so that $\varrho_{3d_{x^2-y^2}} < 0.0033$. ϱ_{3d} is thus almost exclusively in $3d_{z^2}$. Note that $\varrho_{3d} = \alpha_1^2$ and $\varrho_{4s} = \alpha_1''^2$. The remaining spin density making the total to unity is located on the ligands ($\varrho_{lig} = \alpha_1'^2$).

[b] All energies in cm^{-1}.

[c] $\Delta E_4 - \Delta E_3 = \Delta E_1 - \Delta E_2$ is a prerequisite of the analysis (see text).

4.2 The Model Systems

For the $Co^{II}(dmgH)_2$ species observed in frozen water (Fig. 2b) it can be argued that under experimental conditions the Co is six-coordinate (designated M6 in the following). This conclusion is supported by the fact that anhydrous $Co^{II}(dmgH)_2$ is insoluble in non-coordinating inert media and crystallises from oxygen-free aqueous solutions as $Co^{II}(dmgH)_2 \cdot 2H_2O$ [24]. An estimate for the $Co \cdots OH_2$ distance (0.22 nm) and geometry can be gained from the X-ray structural analysis of a similar system (bis(acetylacetonato)Co^{II}) [54]. The existence of such weak six-fold coordinated species is also likely for $Co^{II}(dmgH)_2$ in alcoholic solvents [25 – 28] where the spin Hamiltonian parameters are not much different from those observed in strongly coordinating media like pyridine [27, 28]. In the latter a small hfs from *two* equivalent ^{14}N nuclei was detected along the z-principal axis.

In an isolated four-coordinated complex it may be shown on theoretical grounds (vide supra) that the spin Hamiltonian parameters are markedly different. Schweiger [37] has recently obtained the EPR spectrum of $Co^{II}(dmgH)_2$ in a $Ni^{II}(dmgH)_2$ host, the parameters of which show just this effect. We argue that in the Ni^{II} host, the electronic structure of the $Co^{II}(dmgH)_2$ will very closely resemble that of an isolated four-coordinate complex, designated M4 in the following.

The markedly dissimilar EPR spectra obtained for the Ni^{II} and frozen water hosts, respectively, reflect the different spin Hamiltonian parameters listed in Table 1. Analysing these parameters with particular regard to the energies of the low-lying doublet and quartet excited states (see Table 2), it is noted that for both $^2B_1(xz \rightarrow z^2)$ and $^2B_2(yz \rightarrow z^2)$ an increase of ca. 5000 cm^{-1} occurs, whereas the $^4B_2(xz \rightarrow xy)$ and $^4B_1(yz \rightarrow xy)$ remain essentially unchanged when going from the four- to the six-coordinate model. This may be rationalized as a shift of the d_{z^2} level to higher energy by ca. 5000 cm^{-1} relative to all other d-orbital levels, which remain almost unchanged with respect to one another. This is consistent with simple crystal field arguments. The orthorhombicity of the g tensor in $Co^{II}(dmgH)_2$ reflects the non-cylindrical character of its first coordination sphere in plane. This leads to an energy difference of the d_{xz} and d_{yz} orbitals. The ground state $(d_{z^2})^1$ interacts via spin orbit coupling with excited states involving $(d_{xz})^1$ and $(d_{yz})^1$ occupations with the result that $g_x \neq g_y$. Consequently, the increase of $\Delta E_1(xz \rightarrow z^2)$ and $\Delta E_2(yz \rightarrow z^2)$ upon axial ligation decreases this orthorhombicity owing to the inverse dependence of Δg_x and Δg_y on these energies. In the limiting case of a very strong axial base, like pyridine, the EPR spectra appear to have almost axial symmetry [27], see also [28].

4.3 The Zeolite Species

4.3.1 Precursor species to the superoxo complex (species 1 – 3)

Species 1 which appears in sample A is formed from the smaller proportion of Co^{II} ions already at hand in the supercages; the larger proportion occupy sites in the smaller cages not accessible to the $dmgH_2$ [55], see Figure 1. The EPR spectrum is very similar in appearance to that of M4 with similar g- and ^{59}Co hfs tensors (see Table 1) and linewidth parameters (not given). This points to an absence of axial coordination with water, and also zeolite oxygen atoms, which were postulated to have a coordinative effect similar to that of water in smaller square planar Co^{II} complexes [3]. For all four low-lying excited states (see Table 2), there is good overall agreement with those of M4. Small departures occur for the parameters ϱ_{3d} and ϱ_{4s}. A simple perturbation theory treatment shows that these deviations are quantitatively consistent with a shift of the higher-lying mo of predominantly 4s character (not shown in Fig. 8) to a slightly higher energy relative to the mo's of predominantly 3d character. This may be accounted for by the presence of an additional small, nearly spherical, potential experienced by the Co^{II} from the supercage wall. Species 1 is thus assigned as a structurally undistored four-coordinate $Co^{II}(dmgH)_2$ with the Co^{II} ion centrally located in the supercage.

Species 2 is formed in equilibrium with species 3 after Co^{II} ions are freed from sites in the smaller cages by H_2O. The overall appearance of its EPR spectrum is again similar to that of M4 but the principal g-values and the ^{59}Co hfs values are somewhat modified (see Table 1). Analysis of the spin Hamiltonian parameters yields $^2B_1$, $^2B_2$ energies almost identical to those for M4. The $^4B_1$, $^4B_2$

energies, however, are increased by 8000 – 9000 cm^{-1}, implying a shift in the unoccupied d_{xy} orbital by the same amount. This indicates a distortion of the in-plane crystal field (for axes see Figure 8).

Other possibilities for this species are (i) a dimer [22 – 24] and (ii) a complex with only *one* axially coordinated water molecule. The former case can be safely ruled out in the zeolite hosts for steric reasons. Indisputable five-coordinate square planar complexes of Co^{II} were observed so far only for Co^{II}-porphyrins [56] and related macrocyclic ligands [57], whereas earlier studies postulating five-coordinate $Co^{II}(dmgH)_2$ are questionable on the basis of the measured EPR data [27]. A careful interpolation of the characteristic energy levels and 3d, 4s mo coefficients from the M4 and M6 analysis (Table 2) allows the spin Hamiltonian parameters of a hypothetical five-coordinate complex, with cobalt lying in the basal plane of nitrogen atoms, to be estimated as $g_x = 2.40$, $g_y = 2.22$, $g_z = 2.01$ and $A_x = 220$ MHz, $A_y = 60$ MHz, $A_z = 350$ MHz. These values are similar to those obtained for the THF-adduct of $Co^{II}(dmgH)_2$ that was recently investigated in our laboratory using EPR and ENDOR [28].

For the reasons above, additional axial coordination through a single water molecule or zeolite oxygen would not be expected to yield the species 2 characteristics. It is concluded that species 2 is a four-coordinate $Co^{II}(dmgH)_2$ with a slightly distorted in-plane ligand structure, e.g. as a result of a shortening of the Co···N bonds or an increased charge density at the nitrogen atoms.

Species 3 is also formed under conditions of H_2O infusion and is produced at the expense of species 2. Its EPR spectrum is markedly different in appearance to those of species 1 and 2; the in-plane principal *g*-values lie closer to the free electron *g*-value and the corresponding ^{59}Co hfs values are reduced in magnitude. The spin Hamiltonian parameters yield metal spin density values and excited state energies which are almost the same as those of M6 (see Table 2). This species is therefore assigned as a six coordinate species with two molecules of H_2O occupying the axial positions. Alternatively, one water molecule could be replaced by a zeolite oxygen atom implying that the Co atom is ca 0.22 nm from the wall of the supercage. Steric considerations show that a significant distortion of the in-plane $(dmgH)_2$ frame would be required in such a case. This, in turn, would cause marked deviations from the M6 spin Hamiltonian parameters which are not observed.

In summary, no spectra were observed which could be clearly interpreted as a five-coordinate species with a single, axially-bound water molecule.

4.3.2 Species incorporating O_2 (species 4 – 5)

Species 4 yields spin Hamiltonian parameters typical of those observed for $Co^{III}O_2^-$ species [4]. The principal values of the *g* tensor indicate that it may be viewed as a perturbed O_2^- species; the relatively small ^{59}Co hfs components measured along the principal axes of the *g* tensor (x_{O_2}, y_{O_2}, z_{O_2}, see Fig. 9) are consistent with this description.

Structurally, it is generally found [4] that O_2 is axially coordinated with $r_{Co-O} = 1.9 \pm 0.1$ Å and $r_{O-O} = 1.3 \pm 0.1$ Å, with the O – O bound subtending an angle of $120 \pm 10°$ with the *z*-axis of the Co^{II}

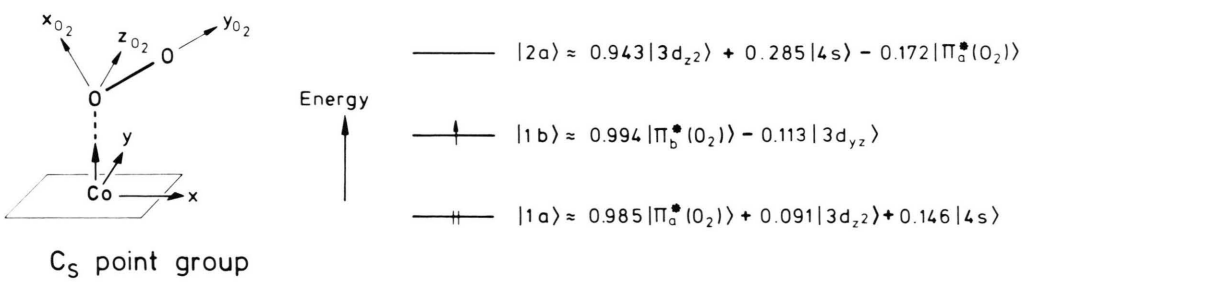

Fig. 9. The three orbital model used for the analysis of the ^{59}Co hfs data. The mo's $|1a\rangle$, $|1b\rangle$, $|2a\rangle$ including their relevant O_2 components $|\pi_a^*(O_2)\rangle$, $|\pi_b^*(O_2)\rangle$ are shown on the right. The molecular axis system (x_{O_2}, y_{O_2}, z_{O_2}) of the cobalt superoxo complex appropriate for the Cs point group is shown on the left. Note that the cobalt orbital components $|3d_{z^2}\rangle$, $|3d_{yz}\rangle$ refer to the axes of the precursor Co^{II} square planar complex, the *y*-axis of which is parallel to z_{O_2}.

precursor and lying in either its xz- or yz plane. To date, only one single crystal EPR/ENDOR study [58] exists, namely for the species vitamin $B_{12r} \cdot O_2$., The similarity of cobaloxime(II) and vitamin B_{12r} has long been recognised [21 – 24]; not surprisingly the g tensor principal values of $B_{12r} \cdot O_2$ and species 4 are very similar. Axis assignment of the principal g values of species 4 (see 3.2.5) was therefore inferred from the $B_{12r} \cdot O_2$ results, with the principal axis for $g_1 \| y_{O_2}$, for $g_2 \| z_{O_2}$, and for $g_3 \| x_{O_2}$. The ^{59}Co hfs tensor is assumed to be collinear with the Co^{II} axis system and therefore non-coincident with the principal axes of the g-tensor.

A consistent interpretation of the spin Hamiltonian parameters has proved difficult for the majority of superoxo species so far measured. The proposal for a spin-polarisation mechanism [59] has, however, allowed an adequate explanation of the anisotropic ^{59}Co hfs components, but the isotropic hfs and the principal g values are largely unexplained. To elucidate the outstanding deficiencies of previous analyses the following procedure has been employed.

Essentially, the 3-orbital model (see Figure 9), proposed by Tovrog *et al.* [59], is retained. The O – O bond is assumed to lie in the xz-plane; the arguments for the yz-plane case are analogous with appropriate interchange of the x, y subscripts. The relevant mo's $|1a\rangle$, $|1b\rangle$, $|2a\rangle$ have the dominant components $\pi_a^*(O_2)$, $\pi_b^*(O_2)$, $3d_{z^2}$, respectively, and are classified according to their transformation properties with respect to the Co – O – O plane of symmetry; a, b correspond to the A', A'' irreducible representations, respectively, of the C_s point group. Spin polarisation effects were then analysed on a more rigorous basis than by Tovrog *et al.* In the 3-orbital scheme with C_S point group symmetry configuration interaction (CI) arguments show that the ground state

$$^2\Psi_0 = |1a\overline{1a}1b|$$

is perturbed by just two singly-excited doublet configurations, and only one of these,

$$^2\Psi'_{1a \to 2a} = \frac{1}{\sqrt{6}} \{2|1a\overline{1b}2a| - |1a1b\overline{2a}| - |\overline{1a}1b2a|\},$$

leads to spin-polarisation. This may be directly estimated by applying perturbation theory to first order (see, for example, equations (12) to (16) in [60]. For the configuration $^2(1a \to 2a)$ the excitation energy was estimated using

$$\Delta E_{^2(1a \to 2a)} = \Delta E_{^2(1a \to 1b)} + \Delta E_{^2(1b \to 2a)} - J_{1a,2a} + J_{1a,1b} + J_{1b,2a} - J_{1b,1b} + \tfrac{1}{2} K_{1a,1b} + \tfrac{1}{2} K_{1b,2a},$$

assuming that $\Delta E_{^2(1a \to 1b)} \approx \Delta E_{^2(1b \to 2a)} \approx 0.5$ eV. The remaining 2-electron Coulomb (J), and exchange (K) integrals, as well as that required for the CI matrix element, were calculated using standard mo procedures.

With the structural information and spin-polarisation outline of the foregoing, the following spin densities giving rise to ^{59}Co hfs were then considered: (i) $3d_{yz}$ spin density (direct admixture), (ii) $3d_{z^2}$ spin density (CI admixture), (iii) 4s spin density (CI admixture), and (iv) localised spin density about each oxygen atom. Both the isotropic and anisotropic ^{59}Co hfs components can be accurately reproduced by this model. Assuming that the relative proportions of $3d_{z^2}$ and 4s in $|2a\rangle$ are identical to those of the corresponding mo of the square-planar Co^{II} precursor, it requires independent $3d_{z^2}$ and 4s components in $|1a\rangle$ and a non-vanishing $3d_{yz}$ component in $|1b\rangle$. The final breakdown of the coefficients for species 4 is that shown in Figure 9. The perturbed ground state was estimated to contain 2.7% admixture of the $^2(1a \to 2a)$ configuration. The quantitative agreement provided by the model shows that the measured ^{59}Co hfs components are dominated by a large negative isotropic part of -37.0 MHz, primarily arising (-33.5 MHz) from CI introduction of negative 4s spin density. This may be traced back to the significant 4s coefficient in the $|1a\rangle$ mo. Secondly, the inevitable close energetic approach of the $|1b\rangle$ and $|2a\rangle$ levels enhances electron- and nuclear spin-orbit coupling effects from the $3d_{yz}$ admixture in $|1b\rangle$, providing significant g-, and ^{59}Co hfs contributions. Finally, our model suggests that within the confines of the 3-orbital restriction ca. 0.9 electrons are transferred to the O_2 moiety, consistent with the formal $Co^{III}O_2^-$ description.

Species 5 is formed under dry conditions after infusion of oxygen (Fig. 6), with simultaneous disappearance of species 1. This species exhibits a weak EPR signal and is not removed or changed by

evacuation. The EPR characteristics led us to assign this species to a nitrogen-based organic radical. The EPR spectrum is not identical to that of the iminoxy radical derived from $dmgH_2$ in a frozen matrix observed by Fox and Symons [61]. However, it could well be a zeolite occluded – immobilised – degradation product of this radical.

4.4 Reaction Sequence

The various paramagnetic intermediates analysed in this work form the basis for gaining a clearer understanding of the chemical processes which take place in the zeolite.

i) The initial condition ($Co_{7.2}NaX$, anhydrous)

After preparation of anhydrous $Co_{7.2}NaX$, Co^{II} ions are distributed amongst tetrahedral sites in the α- and β-cages and octahedral sites in the prisms [45] (denoted by $Co^{II}(T_d, \alpha)$, $Co^{II}(T_d, \beta)$ and $Co^{II}(O_h$, prism), respectively). These species, whose first coordination spheres comprise oxygen atoms, are expected to have $S = 3/2$ ground states [62] and give rise to the broad, low field EPR signal observed.

ii) Introduction of $dmgH_2$ under anhydrous conditions

Owing to the size of the $dmgH_2$ molecule [34] (see Fig. 1) it will reside predominantly – if not exclusively – in the α-cages. The apparent yield of species 1 – undistorted square-planar $Co^{II}(dmgH)_2$ – relative to the total Co^{II} content of $Co_{7.2}NaX$, suggests that the $dmgH_2$ reacts initially with $Co^{II}(T_d)$ in the α-cages. UV/visible spectroscopic studies [33, 34] indicate that complexation of $Co^{II}(T_d, \alpha)$ proceeds as a sequence of distorted tetrahedral intermediates and culminating with unattached $Co^{II}(dmgH)_2$, situated within the α-cages whose dimensions are well-matched to those of the complex. During this sequence one mole of H_2O is produced for every mole of $Co^{II}(dmgH)_2$. This water does not ligate the complex, but diffuses away, presumably to hydrate the lattice walls. Significant aquation of the complex is not promoted; careful inspection of sample A reveals that only trace quantities of species 3 ($Co^{II}(dmgH)_2 \cdot 2\,H_2O$) are present. Furthermore, the H_2O formed does not apparently reach a concentration sufficient to cause a redistribution of the remaining Co^{II}, with a concomitant influx into the α-cages. Under a reduced pressure of argon at room temperature, the EPR spectum (Fig. 3) remains stationary for several months.

iii) Infusion of H_2O

H_2O is expected to diffuse fairly freely throughout the α- and β-cages and prisms of the zeolite lattice. As the concentration of H_2O increases in the zeolite, species 1 – unattached $Co^{II}(dmgH)_2$ – will be hydrated to give $Co^{II}(dmgH)_2 \cdot 2\,H_2O$. Furthermore, there will be a net displacement of Co^{II} ions from β-cages and prims into the α-cages. These Co^{II} will then react with the surfeit of $dmgH_2$ in the presence of H_2O also leading to the diaquo-complex (species 3). As long as the amount of water is limited this species exists together with species 2 – distorted $Co^{II}(dmgH)_2$ – in the zeolite cage. The concentration of species 2 can be considerably decreased by further hydration of the sample with a concomitant increase of species 3 (the diaquo-complex).

The primary difference in the formation of species 1 and 2 is that in the latter case H_2O is simultaneously present. Several models for species 2 can be proposed, *vide supra*. The theoretical analysis of the spin Hamiltonian parameters excluded a five-coordinated species and supports the view that this $Co^{II}(dmgH)_2$ species has a distorted in-plane ligand structure, e.g. by interaction with the zeolite wall. The absence of a five-coordinate complex is surprising, its existence as an intermediate cannot, however, be excluded. In the zeolite matrix – and at the low temperature of the EPR measurements (120 K) – the respective equilibria involved could favour predominantly the four- and six-coordinate species.

iv) Introduction of oxygen

Under aqueous conditions, O_2 reacts rapidly with all $Co^{II}(dmgH)_2 \cdot 2\,H_2O$ to form the superoxo complex (species 4, $Co^{III}(dmgH)_2 \cdot H_2O \cdot O_2^-$), which is stabilized relative to the diaquo complex according to the redistribution of electrons in the valence orbitals. This superoxo-complex is *quite stable* and cannot be removed by evacuation. This contrasts the results obtained in the "dry" case (*vide infra*). A possible explanation lies in the presence of a large excess of H_2O, providing a fifth ligand trans to oxygen and probably also a stabiliz-

ing H-bond between water at the zeolite wall and the β-oxygen atoms in the superoxo complex. Such situations have been discussed for biological systems [63].

A persistent aqueous condition aids the slower conversion of species 2 to the diaquo complex, which then in turn is rapidly converted to the superoxo complex. The involvement of a five-coordinate complex $Co^{II}(dmgH)_2 \cdot H_2O$ as an intermediate is possible although such a species could not be observed under the experimental conditions. At first sight, the absence of the five-coordinate complex is surprising since it is expected that the superoxo complex is formed via this species. An explanation could lie in the existence of a small fraction of a five-coordinate cobalt in equilibrium, especially at higher temperatures. An alternative is the exchange of a water ligand for O_2, i.e. the direct attack of the diaquo complex by oxygen. In aqueous solutions of $Co^{II}(dmgH)_2$, where the complex is six-coordinate, it is known that a different reaction takes place with oxygen, yielding a hydroxy aquo Co^{III} complex [24]. We have no evidence that such a reaction takes place in the zeolite. It can be assumed that a "self destruction" of the complex by such or similar reactions is precluded in the zeolite since the species are held well apart from each other and cannot diffuse together as in normal solution chemistry.

Apparently, the four-coordinate complex present in the hydrated sample does not readily react with oxygen – it also reacts quite slowly with additional water. This could be due to the distorted structure postulated for this complex. The superoxo complex formed in the reaction sequence is only stable as a monomeric species due to its occlusion in the zeolite matrix. Apparently, the latter plays a role similar to the corrin system in vitamin B_{12r}, where a superoxo species could also be observed [22, 23, 58].

Under anhydrous conditions, the effect of infusing excess oxygen is particularly interesting. The EPR signal from the small percentage of Co^{II} ions already in the α-cages and complexed with $dmgH_2$ (species 1) is completely removed and replaced by that of an organic – probability nitrogen-based – radical. A control experiment using Co-absent NaX, but otherwise identical conditions of $dmgH_2/O_2$, yields no EPR signal. These two results strongly suggest that *either* the oxygen forms a transient superoxo-Co^{III} complex, which further attacks the *excess* $dmgH_2$ finally yielding the observed radical and a diamagnetic Co^{III} residue, *or* the oxygen directly attacks the $Co^{II}(dmgH)_2$ whose breakdown itself yields products containing the radical. The first possibility involves the activation of oxygen and might be interesting with respect to potential catalytic function.

5. Conclusions

In this paper the formation of a neutral organometallic complex – $Co^{II}(dmgH)_2$ – within a zeolite X host and its subsequent reactions with water and oxygen were investigated. Our aim was to thoroughly characterise the paramagnetic complexes involved in this reaction sequence using EPR spectroscopy and to compare the results with those obtained from appropriate model complexes in polycrystalline non-zeolite hosts. The identification process was aided by a theoretical analysis of the spin Hamiltonian parameters, allowing the individual ligand-field effects to be compared. Supplementary work on these systems, using ESCA [32] and optical reflectance spectroscopy [33, 34], has been published elsewhere. It should be pointed out that the main conclusions of this paper are corroborated by the optical data [34].

The chemistry in zeolite hosts offers several advantages over that in normal solutions. A complex encapsulated in a supercage may be likened to a "molecular ship in a bottle" [15]. Such species are not free to diffuse around and react with themselves, with solvent or with other species in an uncontrolled manner. Consequently, all complexes are monomeric; dimer formation is not detected (i.e. of μ-oxo complexes) in contrast to solution chemistry [24]. Furthermore, a self-destruction – e.g. of the oxygen-carrying species – is not observed owing to the immobilization and the lack of a reaction partner. Another aspect is the impact of the zeolite upon the electronic structure of the complexes. This can be a direct effect through crystal fields or ligation, or a more indirect one caused by distortions of the existing in-plane or axial ligand structure. Although not very pronounced, all these effects play a certain role in determining the special chemistry of the zeolite-occluded Co^{II} complexes discussed in this paper.

The use of oxo-complexes inside a zeolite offers interesting prospects as selective metal oxidation catalysts. It may be anticipated that such zeolite-occluded species would have an increased lifetime.

It is tempting to compare the zeolite situation with that of metal ions or complexes in a protein host as found in metalloenzymes [64]. Model studies of specific zeolite-occluded species can certainly broaden our understanding of the quite complicated processes in biological systems and might open a way to mimic the natural system.

Acknowledgements

The authors are grateful to Dr. M. Plato (Freie Universität Berlin) for placing his spectral simulation programme at their disposal, to M. Baumgarten (FU Berlin) for helpful discussion concerning the model systems, and to Dr. A. Schweiger (ETH Zürich) for communicating his spectrum of $Co^{II}(dmgH)_2$ in $Ni^{II}(dmgH)_2$ to us. Professors H. Kurreck and K. Möbius (both FU Berlin) are thanked for the use of their equipment. Financial support by the Fonds der Chemischen Industrie (to W.L.) and the DFG (Sfb 161) (to W.L. and C.W.) is gratefully acknowledged.

[1] P. A. Jacobs, N. I. Jaeger, P. Jirù, and G. Schulz-Ekloff (Eds.), Metal Microstructures in Zeolites, Stud. Surf. Sci. Catal. Elsevier, Amsterdam 1982.
[2] R. Kellermann and K. Klier, in Surface and Defect Properties of Solids, Vol. **4**, 1 (1975), Spec. Periodical Reports, Chemical Society.
[3] J. H. Lunsford, Catal. Rev. Sci. Eng. **12**, 137 /1975).
[4] T. D. Smith and J. R. Pilbrow, Coord. Chem. Rev. **39**, 295 (1981), and Refs. cited therein.
[5] P. E. Riley and K. Seff, Inorg. Chem. **13**, 1355 (1974).
[6] J. H. Lunsford and E. F. Vansant, J. Chem. Soc. Faraday II **69**, 1028 (1973).
[7] K. A. Windhorst and J. H. Lunsford, J. Amer. Chem. Soc. **97**, 1407 (1975).
[8] E. F. Vansant and J. H. Lunsford, Adv. Chem. Ser. **121**, 441 (1973).
[9] R. F. Howe and J. H. Lunsford, J. Amer. Chem. Soc. **97**, 5156 (1975).
[10] R. F. Howe and J. H. Lunsford, J. Phys. Chem. **79**, 1836 (1975).
[11] K. Mizuno, S. Imamura, and J. H. Lunsford, Inorg. Chem. **23**, 3510 (1984).
[12] K. Mizuno and J. H. Lunsford, Inorg. Chem. **22**, 3484 (1983).
[13] O. M. Zakharova, B. V. Romanovskii, R. E. Mardaleishvili, and V. Yu. Zakharov, Dokl. Akad. Nauk SSSR **241**, 846 (1978).
[14] R. A. Schoonheydt and J. Pelgrims, J. Chem. Soc. Dalton 914 (1981).
[15] N. Herron, Inorg. Chem. **25**, 4714 (1986).
[16] V. Yu. Zakharov and B. V. Romanovskii, Vestnik Moskovskogo Universiteta, Khimiya **34**, 78 (1979).
[17] G. Meyer, D. Wöhrle, M. Mohl, and G. Schulz-Ekloff, Zeolites **4**, 80 (1984).
[18] Y. Ohgo, S. Takeuchi, Y. Natori, and J. Yoshimura, Bull. Chem. Soc. Japan **54**, 2124 (1981).
[19] S. Németh, Z. Sceverényi, and L. J. Simándi, Inorg. Chim Acta **44**, L107 (1980).
[20] S. Németh and L. J. Simándi, J. Mol. Catal. **14**, 87 (1982).
[21] G. N. Schrauzer, Angew. Chem. **88**, 465 (1976).
[22] G. N. Schrauzer and L. P. Lee, J. Amer. Chem. Soc. **92**, 1551 (1970).
[23] G. N. Schrauzer and L. P. Lee, J. Amer. Chem. Soc. **90**, 6541 (1968).
[24] G. N. Schrauzer and R. J. Windgassen, Chem. Ber. **99**, 602 (1966).
[25] E. K. Ivanova, I. N. Marov, A. T. Panfilov, O. M. Petrukin, and V. V. Zhukov, Zhur. neorg. Khim. **18**, 1298 (1973).
[26] I. N. Marov, A. T. Panfilov, and E. K. Ivanova, Koordinatsionnaya Khimiya **2**, 948 (1976).
[27] A. Rockenbauer, E. Budó-Záhonyi, and L. J. Simándi, J. Chem. Soc. Dalton 1729 (1975).
[28] M. Baumgarten, W. Lubitz, and C. J. Winscom, Chem. Phys. Lett. **133**, 102 (1987).
[29] D. Diegruber, P. J. Plath, G. Schulz-Ekloff, and M. Mohl, J. Mol. Catal. **24**, 115 (1984).
[30] H. Diegruber, R. Möseler, P. J. Plath, W. Lubitz, and C. J. Winscom in R. Sersale, C. Colella, and R. Aiello (Eds.), "Fifth International Conference on Zeolites/Recent Progress Reports and Discussions," Naples 1980, p. 131ff.
[31] C. J. Winscom, W. Lubitz, H. Diegruber, and R. Möseler, in [1], p. 15ff.
[32] J. Strutz, H. Diegruber, N. I. Jaeger, and R. Möseler, Zeolites **3**, 102 (1983).
[33] H. Diegruber, and P. J. Plath in [1], p. 23ff.
[34] D. Diegruber, PhD. Thesis, University of Bremen, West Germany 1984.
[35] D. W. Breck and E. M. Flanigan, Molecular Sieves, Soc. Chem. Ind., London 1968, p. 47.
[36] J. F. Charnell, J. Crystal Growth **8**, 291 (1971).
[37] A. Schwaiger, private communication.
[38] B. Bleaney, Phil. Mag. **42**, 441 (1951).
[39] N. M. Atherton and C. J. Winscom, Inorg. Chem. **12**, 383 (1973).
[40] A. Rockenbauer and P. Simon, J. Magn. Reson. **18**, 320 (1975).
[41] W. Froncisz and J. S. Hyde, J. Chem. Phys. **73**, 3123 (1980).
[42] A. Skorobogaty, T. D. Smith, J. R. Pilbrow, and S. J. Rawlings, J. Chem. Soc. Faraday II **82**, 173 (1986).
[43] H. M. McConnell, J. Chem. Phys. **25**, 709 (1956).
[44] I. D. Mikheikin, O. I. Brotikowskii, G. M. Zhidomirov, and V. B. Kazanskii, Kinetika i Kataliz **12**, 1442 (1971).
[45] I. D. Mikheikin, G. M. Zhidomirov, and V. B. Kazanskii, Russian Chem. Rev. **41**, 463 (1972).
[46] F. A. Cotton and G. Wilkinson, Advanced Inorganic Chemistry, pp. 723 – 724, Interscience, London 1963.
[47] B. R. McGarvey, Can. J. Chem. **53**, 2498 (1975).
[48] C. Daul, C. W. Schläpfer, and A. von Zelewsky, Struct. Bonding **36**, 129 (1979).
[49] T. M. Dunn, Trans. Faraday Soc. **57**, 144 (1961).

[50] A. Abragam and M. H. L. Pryce, Proc. Roy. Soc. London **A206,** 173 (1951).
[51] C. J. Ballhausen, Introduction to Ligand Field Theory, McGraw-Hill, New York 1962, p. 76.
[52] B. R. McGarvey, J. Phys. Chem. **71,** 51 (1967).
[53] E. Clementi, J. Chem. Phys. **41,** 295 (1964).
[54] G. Bullen, Acta Cryst. **12,** 703 (1959).
[55] L. E. Godycki and R. E. Rundle, Acta. Cryst. **6,** 487 (1953).
[56] F. A. Walker, J. Amer. Chem. Soc. **92,** 4235 (1970).
[57] A. Pezeshk, F. T. Greenaway, J. C. Dabrowiak, and G. Vincow, Inorg. Chem. **17,** 1717 (1978).
[58] E. Jörin, A. Schweiger, and Hs. H. Günthard, J. Amer. Chem. Soc. **105,** 4277 (1983).
[59] B. S. Tovrog, D. J. Kitko, and R. S. Drago, J. Amer. Chem. Soc. **98,** 5144 (1976).
[60] C. J. Winscom, Mol. Phys. **28,** 1579 (1974).
[61] W. M. Fox and M. C. R. Symons, J. Chem. Soc. (A) **1966,** 1503.
[62] B. R. McGarvey, in "Transition Metal Chemistry", Vol. 3, R. L. Carlin (Ed.), Marcel Dekker, New York 1966, pp. 90 – 201.
[63] J. Hüttermann and R. Kappl, in "Metal Ions in Biological Systems", H. Sigel (Ed.), Marcel Dekker, New York 1987, Vol. 22, pp. 1 – 80, and Refs. therein.
[64] P. M. Harrison (Ed.), Metalloproteins, Vlg. Chemie, Weinheim 1985, Vol. 1, 2.